Nanoscale

Accepted Manuscript

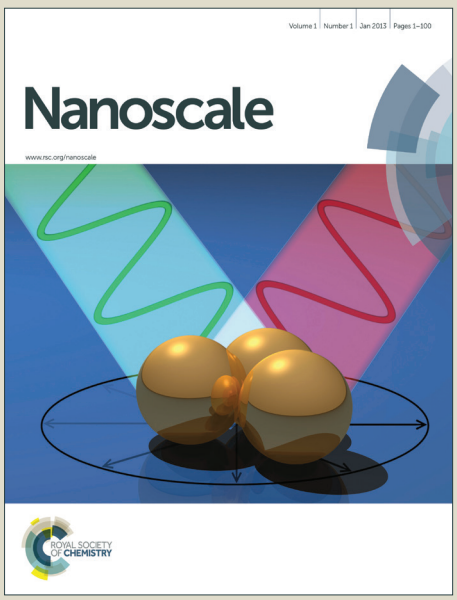

ROYAL SOCIETY OF CHEMISTRY

www.rsc.org/nanoscale

ARTICLE TYPE www.rsc.org/xxxxxx | XXXXXXXX

Integrin-targeted pH-responsive Micelles for Enhanced Anticancer Efficiency *In Vitro* and *In Vivo*

Jinjian Liu,‡[a] Hongzhang Deng,‡ [b, c, d] Qiang Liu,[a] Liping Chu,[a] Yumin Zhang, [a] Cuihong Yang,[a] Xuefei Zhao,[b] Pingsheng Huang,[b] Liandong Deng,[b] Anjie Dong,*[b, c, d] Jianfeng Liu*[a]

Received (in XXX, XXX) Xth XXXXXXXXX 201X, Accepted Xth XXXXXXXXX 201X
First published on the web Xth XXXXXXXXX 201X
DOI: 10.1039/b000000x

Considering the journey of the nanocarriers holistically, which begins from the administration site to the target tissue, looking for simple design that may complete that journney, is the key to bringing more of these nanocarriers into clinical applications. Herein, amphiphilic copolymer cRGDfK-poly(ethylene glycol)-b-poly(2,4,6-Trimethoxybenzylidene-1,1,1-tris(hydroxymethyl) ethane methacrylate) (termed as cRGD-PETM) was synthesized for constructing the multifunctional micelles, which combined enhanced drug loading efficiency, tumor targeting and visual detecting property, controlled intracellular drug release ability, to improve the chemotherapeutic effect *in vivo*. Doxorubicin (DOX) was encapsulated within the cRGD-PETM micelles as a model drug (termed as cRGD-PETM/DOX Ms). The size and morphology of the micelles were characterized systematically. Due to not only the hydrophobic interaction but also π-π conjugate action between DOX molecules and the PTTMA copolymers, the cRGD-PETM/DOX Ms exhibited excellent drug loading capacity. The results of *in vitro* drug release studies indicated that the cumulative DOX release from cRGD-PETM/DOX Ms at pH 5.0 was twice that at pH 7.4. The results of fluorescent microscope analysis showed that the cRGD-PETM/DOX Ms could be internalized by 4T1 and HepG2 cells via receptor-mediated endocytosis with rapid drug release intracellularly, which resulted in commendable cytotoxicity in comparation with free DOX. Furthermore, the *ex vivo* imaging studies represented that the cRGD-PETM/DOX Ms improved the drug accumulation and retention in tumor tissues. The *in vivo* anticancer effect studies demonstrated that the cRGD-PETM/DOX Ms obtained significantly higher therapeutic efficacy with lowest side effects in comparation with free DOX and PETM/DOX Ms. These results highlighted that the multifunctional cRGD-PETM/DOX Ms showed great potential as vehicles for hydrophobic anticancer drug delivery.

1. Introduction

The application of nanotechnology to drug delivery has opened up new opportunities to overcome the limitations of many clinically used anticancer drugs (e.g., doxorubicin, paclitaxel), such as low treatment efficacy and high systemic toxicity. In recent years, various kinds of organic and inorganic nanocarriers have been extensively explored for delivering anticancer drugs to target sites, thereby achieving enhanced therapeutic efficacy and minimized the side effects.[1-4] Self-assembled nanosized micelles formed by amphiphilic block copolymers consisting of a hydrophobic core as a drug reservoir and a hydrophilic protecting shell are considered to be excellent drug carriers by virtue of their passive accumulation in tumor tissue through the enhanced permeability and retention (EPR) effect, increasing drug solubility, prolonging blood circulation and flexible multifunctionality.[5-7] In addition, such micelles as the drug vehicles have also been reported to be safe and biocompatible, which can be dissociated into the original block copolymers after sufficient drug release and be quickly eliminated by filtration through kidneys.[8, 9] However, one practical challenge of the micelles in drug delivery is their poor ability to distinguish the cancerous and healthy cells as well as the unsatisfactory intracellular drug release, which always hampered the efficacy of cancer chemotherapy.[10, 11]

In order to increase the drug accumulation in tumor tissue, one effective approach is to connect targeting ligands that can recognize the specific moiety on cancer cell membrane to the micelles' outer layer, affording active targeting nanocarriers, which can achieve cancer cell-specific internalization via the ligand/receptor-mediated endocytosis.[12-14] The mainly employed targeting ligands include antibodies, peptides and aptamers.[15-19] Arg-Gly-Asp (RGD) peptide is one of the earliest utilized ligands which can specially bind with $\alpha_v\beta_3$ integrins overexpressed in cancer cells and neovasculature.[20-22] However, the linear RGD is often quickly degraded by enzymes in biological environments. In this regard, cyclic-RGD (cRGDfK) peptide was developed by Kessler's group and presented highly selective for $\alpha_v\beta_3$ integrins.[23, 24]

Furthermore, the spatiotemporally controlled release of drugs from micelles is also critical. The premature drug release from the carriers would fail to deliver sufficient drugs to the cancer tissues, leading to low efficacy of cancer chemotherapy.[25, 26] To address this challenge, micelles capable of controlled response to physiological events such as changes in extracellular pH, temperature and reactive oxygen species are particularly useful in

the field of therapeutics and diagnostics.[27-30] Of these stimuli, pH-responsiveness is the most widely used for the responsive drug delivery systems. The pH value of normal tissues is about 7.3-7.5, whereas the pH value in tumor tissues is 6.5-7.2 and the pH value of endosome and lysosome is in a range of 4.0-6.0. Some pH-response bonds such as *cis*-acotinyl, ortho-ester, hydrazine, and acetal have been introduced to form pH-responsive cores of the nanocarriers.[31, 32] In recent years, the cyclic benzylidene acetal group has attracted considerable research interest due to the acid-labile property of acetal group which could cause its hydrolysis in acidic environment.[33-36] Moreover, most hydrophobic drugs such as doxorubicin, taxol and 10-hydroxycamptothecin contain aromatic or cyclic rings. There will be strong π-π interaction between the hydrophobic cyclic benzylidene acetal group of the nanocarriers and the drug molecules, which is beneficial for a higher drug payload.[32, 37-40]

For successful anticancer drug nanocarriers, drug loading, release controlling, tumor targeting and visual detecting, should be considered synchronously, which needed to well construct the nanocarriers to elicit their functions in a spatiotemporally controlled manner. In this study, integrin-targeted pH-responsive amphiphilic copolymer was synthesized by RAFT polymerization, which was able to self-assemble into micelles (as shown in scheme 1) in water solution. The pendant cyclic benzylidene acetal groups endow the micelles with high doxorubicin (DOX) loading capacity and pH-responsive disassembling character. The cRGDfK peptide located on the surface of micelles would specially interact with the $\alpha_v\beta_3$ integrin receptors overexpressed on cancer cells surface and facilitate the internalization of cRGD-PETM/DOX Ms through receptor-mediated endocytosis. The drug delivery efficiency and chemotherapy effect of cRGD-PETM/DOX Ms were evaluated systematically *in vitro* and *in vivo*.

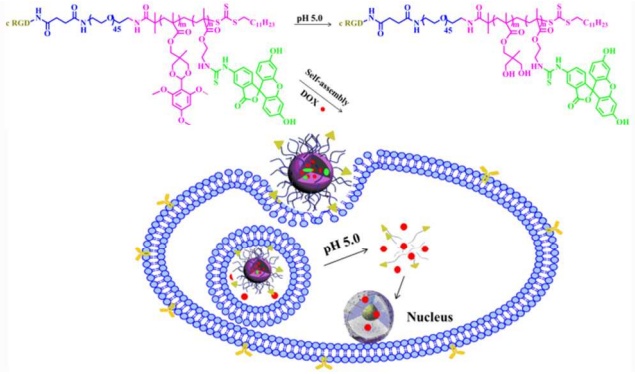

Scheme 1. The schematic illustration of the targeted and pH-triggered delivery of DOX to tumor cells by cRGD-PETM-FITC Ms.

2. Materials and methods

2.1. Materials

The reversible additive fragment transfer agent S-1-dodecyl-S-(R,R-dimethyl-R-acetic acid) trithiocarbonate (DMP) was synthesized as reported.[32] 2,4,6-Trimethoxybenzylidene-1,1,1-tris(hydroxymethyl) ethane methacrylate (TTMA) monomer was synthesized according to our previously reported procedure.[32] 2-Aminoethyl methacrylate hydrochloride(AMA) and trifluoroacetic acid (TFA) were purchased from J&K Scientific Ltd. Methoxy poly (ethylene glycol) Amine (mPEG-NH_2, Mn = 2.0×10^3 g/mol) and Boc-poly (ethylene glycol) Amine (BOC-NH-PEG-NH_2 (Mn = 2.0×10^3 g/mol) were purchased from Beijing JenKem Technology Co., Ltd. Dicyclohexylcarbodiimide(DCC), *N*-Hydroxysuccinimide (NHS), succinic anhydride (SA), fluorescein isothiocyanateand (FITC), and 3-(4,5-Dimethylthiazol-2-yl)-2,5-diphenyltetrazolium bromide (MTT) were purchased from Sigma-Aldrich and used without further purification. Dichloromethane (DCM) and dimethyl formamide (DMF) were purified *via* distillation with CaH_2. Azodiisobutyronitrile (AIBN) was recrystallized in ethyl alcohol before used. Doxorubicin hydrochloride (DOX·HCl) was purchased from Wuhan Hezhong Biochemical in Manufacturing Co., Ltd. cRGDfK was purchased from GL Biochem (Shanghai) Ltd.

2.2. Characterizations

^{1}H NMR (Varian Unity-Plus INOVA 500) was employed to characterize the structure and composition of the monomer and polymers. The number-average molecular weight (*M*n) and polydispersity index (*M*w/*M*n) of copolymers were determined by gel permeation chromatography (GPC) using a Malvern Viscotek GPC max system, which was equipped with a porous styrene-divinylbenzene copolymer-based column (CLM3009, T6000M, General Mixed, Org 300 × 7.8 mm). THF was used as the eluting solvent at a flow rate of 1 mL/min. The diameter and size distribution (PDI) of micelles were measured using Zetasizer 3000HS (Malvern Instrument, Inc., Worcestershire, U.K.) at a wavelength of 633 nm with a constant angle of 173°. Morphologies of micelles were observed under a Hitachi H600 transmission electron microscopy (TEM) system at operated voltage of 100-200 kV.

2.3. Preparation of PETM and cRGD-PETM copolymers

As illustrated in Scheme 2, the PETM and cRGD-PETM copolymers were prepared by two major steps, which were composed of the synthesis of macromolecular RAFT chain transfer agent and polymerization. PETM copolymers were synthesized via RAFT copolymerization of TTMA and AMA, with mPEG-DMP as the RAFT chain transfer agent. Typically, mPEG-DMP (235 mg, 0.1 mM), TTMA (549 mg, 1.5 mM), AMA (16.5 mg, 0.1 mM) and AIBN (3.28 mg, 0.02 mmol) were dissolved in 2 mL of DMF. After three freeze-pump-thaw circles of degassing, the polymerization was conducted at 70 ℃ of oil bath for 24 h. Then, the solution of PETM copolymer was dialyzed against distilled water for 48 h. Furthermore, three different PETM copolymers containing different compositions of TTMA were prepared as shown in Table 1. Then, PETM copolymer was obtained via lyophilization. cRGD-PETM copolymer was obtained with the same polymerization process. The detail method was as follows:

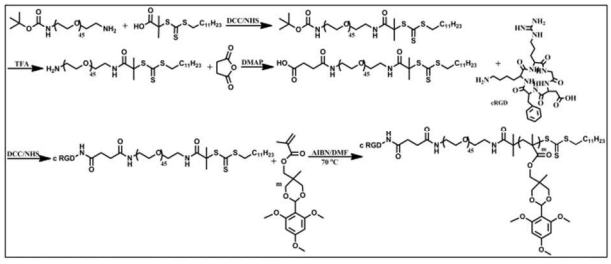

Scheme 2. The synthetic route of cRGD-PETM copolymers.

Preparation of FITC-labeled PETM and cRGD-PETM copolymers was displayed as Scheme 3. In detail, PETM (200 mg, 0.025 mM) and FITC (19.4 mg, 0.05 mM) were co-dispersed in 3 mL DMF under the protection of nitrogen and stirred for 24 h at room temperature. After that, the reaction solution was dialyzed (MWCO: 3500 Da) against distilled water for 72 h to remove the unconjugated FITC completely. Then, PETM-FITC copolymer was obtained via lyophilization. cRGD-PETM-FITC copolymer was obtained with the same method.

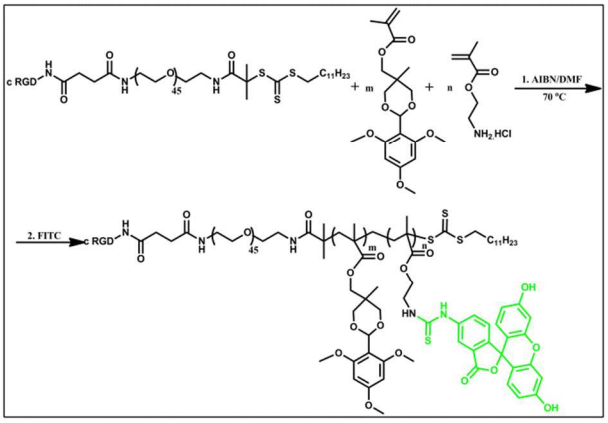

Scheme 3. Preparation of FITC-labeled cRGD-PETM (cRGD-PETM-FITC) copolymers

2.4. Critical micellar concentration (CMC) measurement

The CMC was detected by a steady state fluorescent-probe methodology using Varian Fluorescence Spectrophotometer at room temperature with pyrene as probe.[41] The concentration of copolymers was varied from 10^{-6} to 0.1 mol/L and the concentration of pyrene in the copolymers was 6×10^{-7} mol/L. These solutions were shaken for 12 h and then equilibrated for 24 h at room temperature. The pyrene excitation spectra of the samples were measured (the detection emission wavelength was 373 nm). The CMC value was obtained from the intersection of the tangent to the horizontal line of I_{337}/I_{333} with relative constant value and the diagonal line with rapidly increased I_{337}/I_{333} ratio.[42]

2.5. Preparation and characterisation of polymeric micelles

DOX·HCl (100 mg) was dissolved in 10 mL of borax buffer solution (pH 9.0) and stirred for at least 12 h at room temperature. Then the DOX solution was centrifuged at 10000 rpm for 10 min at 25 °C to obtain the precipitate, which was then washed by pure water to remove any residual borax salt. Eventually, the precipitate was lyophilized to obtain the base form of DOX.

The blank and drug loaded micelles were prepared through dialysis method.[43] Briefly, copolymers (PETM or cRGD-PETM) (10 mg) and DOX (1 mg) were both dissolved in 1 mL of DMF. Then the organic phase was slowly added dropwise into PBS (pH = 7.4) and stirred for another 2 h, following by the extensively dialysis against distilled water for 48 h to remove the DMF and the un-trapped DOX. The blank micelles were prepared as above methods without addition of DOX.

Subsequently, the drug loading content (DLC) was determined by UV-visible spectrophotometer (Biowave II $^{+}$, UK) and then the drug loading efficiency (DLE) was calculated. A standard curve was drawn using different concentrations of DOX (1−50 μg/mL) in TFE. DLC and DLE were calculated from the following equations: [44]

$$\mathrm{DLC}\,(\%) = \frac{\text{weight of loaded drug}}{\text{weight of drug - loaded micelles}} \times 100\% \quad \text{-------[1]}$$

$$\mathrm{DLE}(\%) = \frac{\text{weight of loaded drug}}{\text{weight of drug in feed}} \times 100\% \quad \text{-------[2]}$$

2.6. pH-sensitivity of PETM Ms

The hydrolysis of TTMA in PETM copolymer was determined by UV/vis spectroscopy. Specifically, 1 mg/mL of PETM Ms solution in 0.01 mM PBS (pH 7.4) was prepared, then samples of the PETM Ms solution with pH of 6.0 and 5.0 were obtained by adding 1 N HCl solution dropwise. The samples were then equilibrated for 2 h at room temperature before performing the UV/vis spectroscopy at 292 nm.

2.7. *In vitro* drug release studies

The release behavior of DOX from the PETM Ms was performed in pH-adjusted 0.01 M PBS media at 37 °C under slow shaking, i.e. ,(1) pH 7.4, (2) pH 6.0, and (3) pH 5.0. 10 mL of the DOX-loaded micelles whose pH were adjusted to 6.0 or 5.0 or maintained 7.4 were sealed in a dialysis tube (M_n = 3500). At designate time intervals, 10 ml of the release media was taken out and the amount of drug released was quantified by UV-Vis spectrophotometer. At the same time, equal volume of fresh media was replenished to the release system. The cumulative DOX release percentage was calculated according to the following equation: [44]

$$Er\ (\%) = \frac{V_t\sum_{1}^{n-1} C_i + V_0 C_n}{m_{DOX}} \times 100\% \text{-------[3]}$$

Where m_{DOX} is the amount of DOX encapsulated in the PETM Ms, V_0 represents the volume of the release media (V_0 = 45 mL), V_t is the volume of the replaced media (V_t = 10 mL), and C_n represents the concentration of DOX in the sample.

2.8. *In vitro* cytotoxicity assay

The biocompatibility of blank PETM and cRGD-PETM Ms and the cytotoxicity of free DOX, PETM/DOX and cRGD-PETM/DOX Ms were evaluated by the MTT assay with NIH 3T3, HepG2 and 4T1 cells. In brief, 100 μL of cells suspension was seeded in 96-well plates at a density of 1×10^5 cells/mL and incubated for 24 h at 37°C in a humidified incubator. For the cytotoxicity assay of blank PETM Ms or cRGD-PETM Ms, the cell culture medium was discarded and 100 μL of fresh culture medium containing different concentrations (0, 0.001, 0.01, 0.5 and 1 mg/mL) of blank micelles was added. For the cytotoxicity assay of free DOX or DOX-loaded micelles, the cell culture medium was replaced by fresh medium containing different concentrations of DOX or DOX-loaded micelles, based on the DOX concentrations of 0, 0.06, 0.6, 1.5, 3.0, 6.0 and 16.0 μg/mL. After incubation for 48 h, 25 μL per well of MTT stock solution (5 mg/mL in PBS) were added and incubated for 4 h. The MTT-containing medium was then removed and replaced by 150 μL of DMSO. After 10 min of shaking in the dark, the absorbance at

570 nm was detected with a microplate reader (Varioskan Flash, Thermo, USA).

2.9. *In vitro* cellular uptake

The internalization of blank micelles and DOX-loaded micelles was studied toward NIH 3T3 and HepG2 cells. Briefly, 1mL of cells suspension was seeded in 24-well plates at a density of 1×10^5 cells/mL and incubated for 24 h at 37°C in a humidified incubator. The incubation medium was discarded and then replaced by 1 mL of fresh medium containing PETM-FITC Ms, cRGD-PETM-FITC Ms or 10 μg/mL of free DOX, or equivalent DOX containing PETM/DOX Ms or cRGD-PETM/DOX Ms. 4 h later, the incubation medium was discarded and cells were washed once with PBS and then fixed with 4% paraformaldehyde for 30 min. Then cell nucleus were stained with 1 μg/mL of 4,6-diamidino-2-phenylindole (DAPI) for 15 min at room temperature. The cellular uptake was visualized using an inverted fluorescence microscope (Leica AF 6500). The fluorescence of FITC, DAPI and DOX were observed under an excitation wavelength of 488 nm, 358 nm, 480 nm and emission wavelength was 525 nm, 461 nm and 596 nm, respectively.

2.10. *Ex vivo* drug distribution and tumor accumulation

BALB/c mice (male, 4–6-weeks-old) were purchased from Vital River Laboratories (Beijing, China). All animal procedures were performed according to the guidelines of Administration of Experimental Animals (Tianjin, revised in June 2004). 4T1 cells (1×10^7) suspended in PBS buffer were subcutaneously injected into the right flank of mice to produce breast cancer xenografts. When tumor volume reached approximately 300 mm^3, free DOX, PETM/DOX Ms, cRGD-PETM/DOX Ms were administrated *via* the tail vein at an equivalent DOX dose of 10 mg/kg body weight (n=3). 1, 4 and 8 h after, mice were sacrificed and the main organs (heart, liver, spleen, lung, kidney) and tumor were harvested and immediately scanned by the Kodak IS *in vivo* FX imaging system.

2.11. *In vivo* antitumor activity

The *in vivo* antitumor efficiency of PETM/DOX and cRGD-PETM/DOX Ms was evaluated on 4T1 breast cancer-bearing mice. When tumor volume reached about 200 mm^3, mice were randomly assigned to four treatment groups (n=8): PBS, free DOX, PETM/DOX Ms, cRGD-PETM/DOX Ms. Free DOX, or equivalent DOX containing PETM or cRGD-PETM Ms (with DOX dosage of 5 mg/kg/dose body weight) in 200 μL of PBS solution were injected via the tail vein every two days for five total administrations. The two perpendicular diameters of tumor were measured with vernier calipers every other day and tumor volume were calculated by the formula: tumor volume (mm^3) = (length×width^2)×1/2. The survival of mice was observed continuously.[45]

2.12. Histomorphological analysis

Histopathology of tumor and normal tissues were analysed by hematoxylin and eosin (H&E) assay. Specifically, liver, spleen, kidney and tumor were collected and fixed in 4% paraformaldehyde for 24 h, then tissue samples were trimmed, dehydrated, embedded in paraffin. The samples were cut into 8-μm-thick sections for H&E assay. Photos were taken on optical microscope (Leica DMI6000 B, Germany).

2.12. Statistical analysis

All statistical analysis was performed using SPSS 16.0 software. The statistical significance of differences was determined by one-way analysis of variance (ANOVA). All statistical tests were two-sided, and $^{*}p < 0.05$ and $^{**}p < 0.001$ were used in this study to show statistical significance. The results are shown as mean ± standard deviation.

3. Results and discussion

3.1. Synthesis and characterization of PETM and cRGD-PETM copolymers

Firstly, macromolecule RAFT reagent mPEG-DMP was prepared by the esterification reaction of mPEG and DMP. With mPEG-DMP as RAFT chain transfer agent, mPEG-b-P(TTMA-co-MAA) copolymer was obtained by RAFT copolymerization of TTMA and MAA. Furthermore, cRGD-PEG-b-P(TTMA-co-MAA) copolymer was prepared by the similar procedure, just using the cRGD-mPEG. The chemical structures and compositions of mPEG-b-P(TTMA-co-MAA) and cRGD-PEG-b-P(TTMA-co-MAA) were characterized with ^{1}H NMR and GPC. As shown in Fig 1, it could be seen that the mPEG-b-P(TTMA-co-MAA) had characteristic peaks of both PEG and TTMA. For example, the sharp single peak at 3.63 ppm was attributed to the methylene protons of the PEG. Peaks at 1.42, 1.65, 2.32, and 6.1 ppm were assigned to methylene protons in TTMA units, respectively. The ratio of TTMA and MAA in mPEG-b-P(TTMA-co-MAA) was controlled by adjusting the feed ratio of TTMA to MAA (Table 1). The number of repeating units of TTMA and molecular weight of mPEG-b-P(TTMA-co-MAA) were calculated according to the integral areas of characteristic peaks of ethylene protons (-CH_2-CH_2-O-, at 3.63 ppm) of PEG, benzene ring (at 1.65 ppm) of TTMA units, methyl (-C(CH_3)=C(CH_3)-, at 1.84 ppm). The molecular weight (Mn) and polydispersity index (Mw/Mn) of mPEG-b-P(TTMA-co-MAA) were determined by ^{1}H NMR and GPC, and summarized in Table 1. The molecular weight (Mn) and composition of mPEG-b-P(TTMA-co-MAA) obtained from ^{1}H NMR spectrum approximated to the theoretical values. As shown in Fig 2A, the GPC traces of the mPEG-b-P(TTMA-co-MAA) copolymers all showed a unimodal peak, which confirmed the monomodal molecular weight distribution of the mPEG-b-P(TTMA-co-MAA) copolymers. The Mn of mPEG-b-P(TTMA-co-MAA) copolymers obtained by GPC were higher than those calculated by ^{1}H NMR. This may be ascribed to that the GPC characterizations of the samples were carried out using polystyrene as standards.[46] The $mPEG_{45}$-b-P($TTMA_{15}$-co-MAA_3) was used in vitro and in vivo studied.

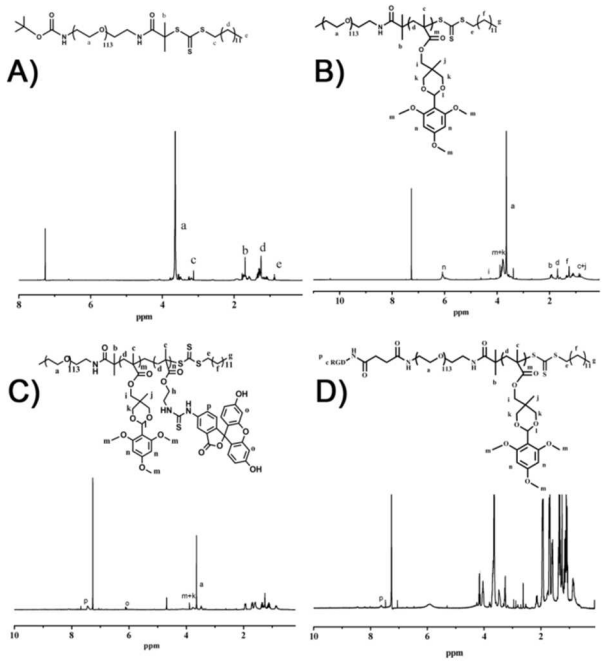

Fig. 1. [1]H-NMR spectra of mPEG-DMP (A), mPEG-b-P(TTMA-co-MAA) (B), mPEG-b-P(TTMA-FITC) (C), and cRGD-PEG- b-P(TTMA-co-MAA) (D).

Table 1. Structure and composition of mPEG-b-P(TTMA-co-MAA)

Polymers[a]	M_n (g/mol)			M_W/M_n[b]
	Theory	^{1}H NMR	GPC[b]	
$mPEG_{45}$-b-P($TTMA_{10}$-co-MAA_3)	6608	5430	7900	1.27
$mPEG_{45}$-b-P($TTMA_{15}$-co-MAA_3)	8003	6958	10000	1.36
$mPEG_{45}$-b-P($TTMA_{20}$-co-MAA_3)	9958	8148	13000	1.25

a The composition calculated from ^{1}H NMR of $mPEG_{45}$-b-P($TTMA_{10}$-co-MAA_3).

b MW/Mn measured by GPC

3.2. Preparation and characterization of micelles

PETM and cRGD-PETM Ms were obtained by a solvent exchange method. Laser particle size analyzer measurements showed that mPEG-b-P(TTMA-co-MAA) copolymers self-assembled into monodisperse micelles of about 130 nm with a low PDI of around 0.2 (Table 2 and Fig 2B). TEM examination was then performed to study the morphology of the micelles. As shown in Fig 2C and Fig 2D, TEM images indicated that mPEG-b-P(TTMA-co-MAA) and cRGD-PEG-b-P(TTMA-co-MAA) both formed homogeneous spherical micelles with diameter of around 120 nm.

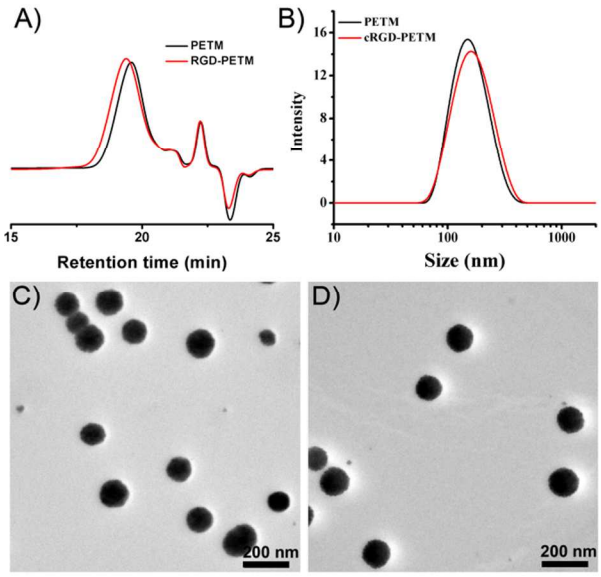

Fig. 2. Characterization of PETM and cRGD-PETM copolymers and Ms. GPC traces of PETM and cRGD-PETM copolymers (A), Laser particle size of PETM and cRGD-PETM Ms (B), TEM of PETM Ms (C) and cRGD-PETM Ms (D). The scale bar was 200 nm.

The CMC of copolymers was characterized by fluorescence technique based on pyrene probe. The absorption shift from 333 to 337 nm of pyrene in $mPEG_{45}$-b-P($TTMA_{15}$-co-MAA_3) copolymer in the excitation spectrum happened with increased polymeric micelle concentration reflected the change in environmental polarity (Fig 3A). As shown in Fig 3B and Table 2, according to the ratio of pyrene fluorescence intensity at 337 nm to that at 333 nm plotted against the logarithm of copolymer concentrations, the CMC could be obtained, which is measured to be 1.2×10^{-3} mg/mL for $mPEG_{45}$-b-P($TTMA_{15}$-co-MAA_3).

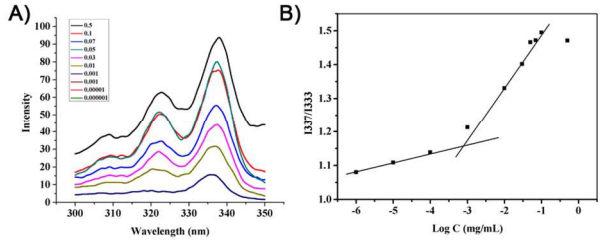

Fig. 3. Emission spectrum for aqueous solutions of PETM (A) and plot of I_{337}/I_{333} in the excitation spectrum versus the concentrations of copolymers in aqueous solution (B).

3.3. pH-triggered dissociation of PETM Ms

The pH-sensitivity of PETM Ms was realized by the hydrolysis of cyclic benzylidene acetals in PETM copolymers and the hydrolysis was investigated at acidic pH of 5.0 and 6.0 and the physiological pH of 7.4 at 37 °C. As shown in Fig 4, the absorbance of 292 nm increased as the pH decreased to 6.0 and 5.0 at all the time points within 12 hours, which was consistent with the previous report.[32] These results indicated that the hydrolysis of acetals in PETM copolymer was highly pH-dependent and this should contribute to the stability of PETM Ms under physiological conditions and its degradation in the acid tissues, for instance, tumor tissue, and thus the

diffusion of the loaded drugs.

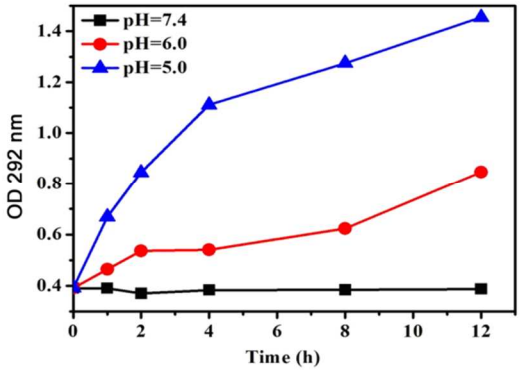

Fig. 4. Hydrolysis kinetics of PETM Ms at pH 7.4, 6.0 and 5.0.

3.4. DOX encapsulation and *in vitro* pH-triggered release

DOX, as a model drug of tumor chemotherapeutic therapy, was empolyed to evaluate the properties of PETM Ms as a drug carrier. DOX-loaded PETM Ms (PETM/DOX Ms) were prepared with polymer concentration of 1 mg/mL. The drug encapsulation efficiency, drug loading content, micelles size and size distribution were summarized in Table 2. The micelles size increased to a varying extent as the number of repeating units of TTMA in PETM changed. Interestingly, the drug loading efficiency of PETM Ms increased with increasing the molecular weights of P(TTMA) segments. This phenomenon might be due to the π-π interation between benzene ring of PTTMA and DOX which was in favor of DOX loading.[47]

Table 2. Characteristics of PETM and PETM/DOX Ms

Copolymers	PETM Ms			PETM/DOX Ms [c]			
	Size (nm)[a]	CMC (mg/mL)[b]	PDI[a]	Size (nm)[a]	PDI[a]	DLC (%)	DLE (%)
mPEG$_{45}$-b-P(TTMA$_{10}$-co-MAA$_3$)	115 ± 11	0.1×10^{-3}	0.17	109 ± 8	0.17	4.7	31
mPEG$_{45}$-b-P(TTMA$_{15}$-co-MAA$_3$)	136 ± 13	1.2×10^{-3}	0.20	120± 14	0.16	5.6	37
mPEG$_{45}$-b-P(TTMA$_{20}$-co-MAA$_3$)	145 ± 9	3.2×10^{-3}	0.11	137± 15	0.13	7.9	53

[a] Determined using laser particle size (zetasizer Nano ZS, Malvern Instruments) at 25 °C in PBS (10 mM, pH 7.4).

[b] measured by a fluorescence technique with pyrene as a probe.

[c] Feed ration of DOX to polymers was 15 mg/100 mg.

CMC: critical micellar concentration; PDI: the size and size distribution; DLC: the drug loading content; DLE: drug loading efficiency.

The *in vitro* drug release profiles were performed on PETM/DOX Ms at pH 7.4, 6.0 and 5.0 with polymer concentration of 1 mg/mL. As shown in Fig 5, the drug release rate of PETM/DOX Ms was clearly pH dependent. In comparison to the release profile at psychological pH (7.4), the release of DOX from PETM/DOX Ms was significantly enhanced at pH 5.0, which could be attributed to the hydrolysis of TTMA resulting in the swell and disassembly of the micelles (Fig 4). This result indicated that the drug release could be restrained at pH 7.4 in the blood stream, however, fast release would be realized upon endocytosis due to the acid microenvironment in the endo/lysosomal compartments (pH = 4.0~6.0).[48]

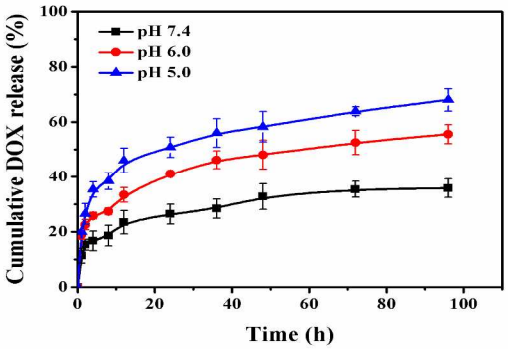

Fig. 5. *In vitro* release of DOX from PETM Ms at pH 7.4, 6.0 and 5.0.

3.5. Celluar toxicity and *in vitro* cancer targeting studies

The cellular toxicities of blank PETM and cRGD-PETM Ms were evaluated by MTT assays towards NIH 3T3 and HepG2 cells. As show in Fig 6A and 6B, the viabilities of both NIH 3T3 and HepG2 cells were higher than 90% even when the concentration of PETM and cRGD-PETM Ms reached to 1 mg/mL. And there had no statistical difference between the PETM and cRGD-PETM Ms in cell viabilities. This indicated that the modification of cRGDfK would not affect the biocompatibility of PETM Ms and that both PETM and cRGD-PETM Ms could be safely used as drug carriers with very high concentration.

Because both PETM and cRGD-PETM Ms were labeled with FITC, we could observe the distribution and relative amount of micelles entered the cells by fluorescence observation. As shown in Fig 6C, the fluorescence intensity was weak and could not identify the difference between PETM and cRGD-PETM Ms for normal NIH 3T3 cells. In comparison, the fluorescence intensity of HepG2 cells incubated with cRGD-PETM Ms was much higher than that incubated with the micelles without cRGDfK conjugation. As HepG2 cells were reported to overexpress $\alpha_v\beta_3$ integrins, these results revealed that cRGD-PETM Ms could be more effectively internalized by the integrin overexpressed HepG2 cells through the ligand/receptor mediated endocytosis.

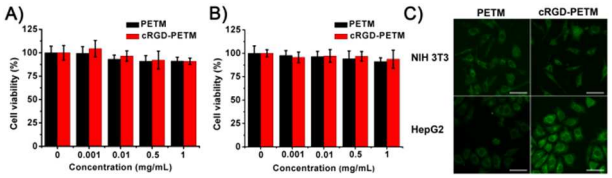

Fig. 6. Cell viability of PETM and cRGD-PETM Ms on NIH 3T3 cells (A) and HepG2 cells (B) for 48 h, data were presented as mean ± standard deviation (n=8). And the inverted fluorescence microscope images of NIH 3T3 and HepG2 cells after incubation with PETM-FITC and cRGD-PETM-FITC Ms for 4 h (C). The scale bar was 25 μm.

3.6. Cellular uptake and proliferation inhibition

To further verify the *in vitro* cancer cell targeting capability of the cRGD-PETM Ms, the cellular uptake of DOX from free DOX, PETM/DOX and cRGD-PETM/DOX Ms were examined using inverted fluorescence microscope toward the

normal NIH 3T3 cells and two kinds of 4T1 and HepG2 cancer cells. As could be seen from Fig 7A, the intensity of DOX fluorescence in normal NIH 3T3 cells incubated with cRGD-PETM/DOX Ms was weak and the fluorescence intensities had almost no difference between the cells incubated with cRGD-PETM/DOX and PETM/DOX Ms. This result indicated that the modification of targeting peptide cRGDfK could not improve the intracellular uptake of micelles to the $\alpha_v\beta_3$ integrin low expressed NIH 3T3 cells. By contrast, stronger DOX fluorescence intensities were observed in both 4T1 and HepG2 cancer cells incubated with cRGD-PETM/DOX Ms than those of cells incubated with PETM/DOX Ms (Fig 7C and 7E). This result further demonstrated the active targeting ability of cRGD-PETM/DOX Ms to $\alpha_v\beta_3$ integrin overexpressed cancer cells.

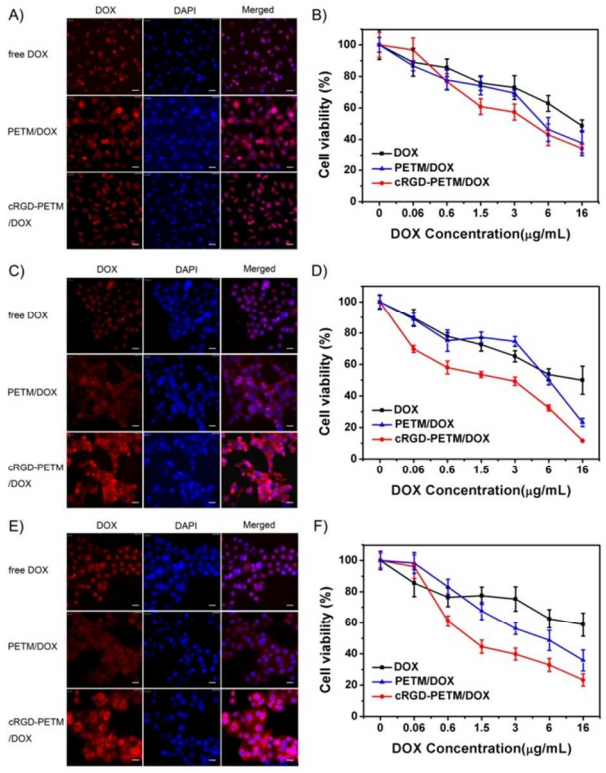

Fig. 7. Inverted fluorescence micrographs of NIH 3T3 cells (A), 4T1 cells (C) and HepG2 cells (E) incubated with free DOX, PETM/DOX Ms and cRGD-PETM/DOX Ms for 4 h at 37 ℃. (Red and blue represented the fluorescence of DOX and DAPI, respectively). Cell viability of free DOX, PETM/DOX Ms and cRGD-PETM/DOX Ms to NIH 3T3 cells (B), 4T1 cells (D) and HepG2 cells (F) after incubation for 48 h. Data are presented as mean ± standard deviation (n=8). The scale bar was 25 μm.

The effects of DOX-loaded targeted cRGD-PETM Ms and non-targeted PETM Ms as well as free DOX on the proliferative ability of NIH 3T3, 4T1 and HepG2 cells were studied by MTT assay at 48 h post-treatment. As depicted in Fig 7B, free DOX had no selectivity to the normal and cancer cells, as evidenced by the similarly 50%-60% cell viabilities to all three kinds of cell lines (at a Dox concentration of 16 μg/mL dose). This result agreed well with the serious side effect of DOX in the clinical application. The targeted cRGD-PETM Ms showed higher growth inhibition than PETM Ms to 4T1 cells (11.63±0.47% versus 23.14±2.61%) (Fig 7D) and HepG2 cells (23.26±3.94% versus 35.84±6.71%) (Fig 7F) at 16 μg/mL dose of DOX. The high cytotoxicity exhibited by the targeted cRGD-PETM Ms should be attributed to their high level of cellular uptake in comparison to that of the non-targeted PETM Ms in 4T1 and HepG2 cells, which was confirmed by the cellular uptake studies (Fig 7C and 7E). As expected, the proliferative ability of NIH 3T3 cells treated with cRGD-PETM/DOX Ms and PETM/DOX Ms had no significant difference (44% versus 48%) (Fig 7B). This results were in accordance with the cellular uptake results, in which the DOX fluorescence intensity in NIH 3T3 cells treated with cRGD-PETM/DOX and PETM/DOX Ms was relatively weak and almost the same.

3.7. *Ex vivo* drug distribution and tumor accumulation

To directly visualize the differences in the biodistribution and the tumor accumulation of the micelles with and without cRGDfK functionalization, free DOX, PETM/DOX and cRGD-PETM/DOX Ms were injected intravenously into BALB/c mice bearing 4T1 tumor xenografts, respectively. Subsequently we monitored the fluorescence intensities of DOX in tumor and major organs including heart, liver, spleen, lung, kidney at designated time intervals by *ex vivo* imaging. As shown in Fig 8, as compared to free DOX group, both PETM/DOX and cRGD-PETM/DOX Ms increased the accumulation of DOX in tumor, which should be caused by the passive targeting of micelles through the EPR effect. Furthermore, the cRGD-PETM/DOX Ms group displayed significantly higher fluorescence intensity in tumor tissue than PETM/DOX Ms group at all the tested time points. These results suggested that the drug delivery system with the cRGD functionalized micelles presented much better specificity to target tumor *in vivo*.

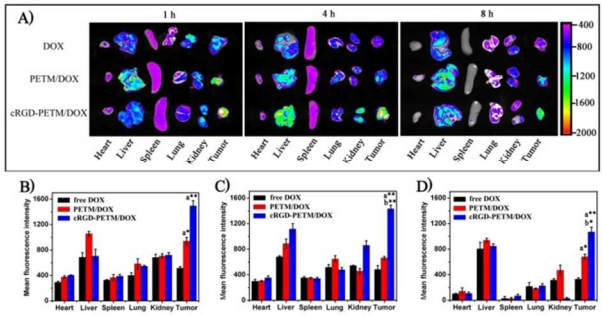

Fig. 8. (A) Fluorescence images of major organs and tumor after administration of free DOX, PETM/DOX Ms and cRGD-PETM/DOX Ms at 1, 4 and 8 h. Quantitative analyses of mean fluorescence intensities of DOX in the organs and tumor at 1 h (B), 4 h (C) and 8 h (D) (a=in comparation with free DOX, b=in comparation with PETM/DOX Ms, *p<0.05, **p<0.01). The data were expressed as mean ± standard deviation, n = 3.

3.8. *In vivo* antitumor activity evaluation

The *in vivo* antitumor activities of PETM/DOX and cRGD-PETM/DOX Ms were studied using a 4T1 xenograft model in BALB/c mice. The animals were randomly grouped into PBS, DOX, PETM/DOX Ms and cRGD-PETM/DOX Ms,

respectively, based on the same dose of DOX by intravenous injection. As shown in Fig 9A, the tumor volumes treated with free DOX and two Dox-loaded micelle groups were much smaller than that of PBS group. At the same time, PETM/DOX and cRGD-PETM/DOX Ms had better antitumor activity than free DOX, and cRGD-PETM/DOX Ms had significantly higher antitumor effect than PETM/DOX Ms. This result was consistent with that of DOX accumulationin tumor tissue for various treatment groups. As depicted in Fig 8A PETM/DOX and cRGD-PETM/DOX Ms groups had higher DOX concentration in tumor through the passive targeting of EPR effect of micelles and cRGD-PETM/DOX Ms group had higher DOX concentration in tumor than PETM/DOX Ms group by the active targeting of cRGDfK peptide. Fig 9B showed the survival curve of tumor bearing BALB/c mice receiving various treatments, it could be seen that the mice treated with cRGD-PETM/DOX Ms had the longest survival rate, which was followed by PETM/DOX Ms group and free DOX group. The tumor volume and survival results indicated that the better inhibition of tumor volume could bring longer survival time of mice.

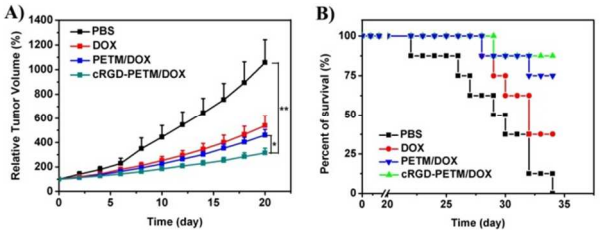

Fig. 9. *In vivo* antitumor effect of free DOX and DOX-loaded micelles to BALB/c mice at the dose of 5 mg/kg/dose body weight for five doses. (A) Relative tumor volume of different treatment groups (n=8), the data were expressed as mean ± standard deviation (*p<0.05, **p<0.01), and (B) Survival rate of mice over time during various treatments.

3.9. Histomorphological analysis

H&E assays were executed to study the toxicology and the antitumor efficacy of the DOX-loaded PETM and cRGD-PETM Ms. Liver and spleen are the reticuloendothelial system (RES) organs and the nanosized materials preferentially distribute in these organs after intravenous injection. Kidney is the elimination organ of most micelles. Hence, liver, spleen and kidney were collected for the *in vivo* toxicity studies. H&E results showed in Fig 10 suggested that there were no pathological changes in liver, spleen and kidney in both PETM/DOX and cRGD-PETM/DOX Ms groups, indicating the safety of our DOX loaded micelles *in vivo*. The breast cancer xenograft images in Fig 10 revealed that the largest area of apoptotic or necrosis cells (with broken nucleis) was found in cRGD-PETM/DOX Ms group, which was in accordance with the best *in vivo* antitumor effect of cRGD-PETM/DOX Ms in Fig 9A. These results indicated clearly that the tumor inhibition ability of DOX was significantly enhanced by tumor-targeted cRGD-PETM Ms encapsulation.

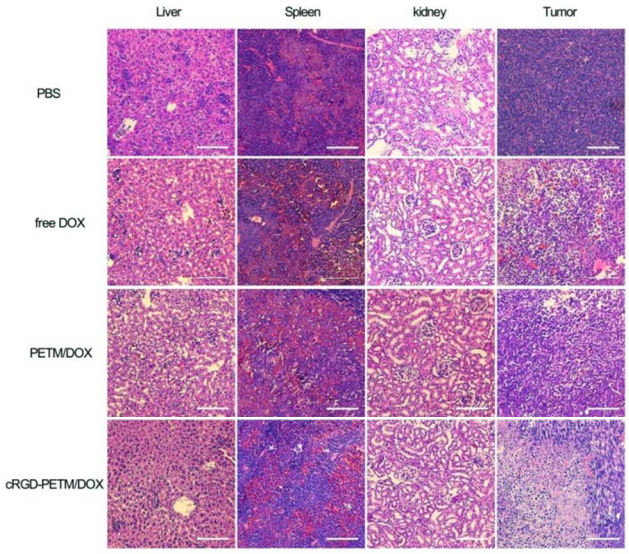

Fig. 10. Hematoxylin & eosin (H&E) assays of tumor and organs (liver, spleen and kidney) from mice that received different treatments. The scale bar was 50 μm.

4. Conclusion

In summary, we have designed and synthesized the cRGD-PETM copolymer, which could self-assemble into nanosized micelles for intelligent antitumor drug delivery. The cRGDfK peptide functionalization allows the micelles for active tumor targeting and the pH-sensitive cyclic benzylidene acetal groups in the core rendered the micelles with ability for pH-triggered and controlled DOX release. The cRGD-PETM Ms had good biocompatibility and could preferentially cleavable in tumor tissues and stable in blood plasma, thus the pH-triggered release of the payloads is realized only under acidic tumor environment. The cRGD-PETM Ms exhibited a much higher cellular uptake in cancer cells and higher accumulation in tumor tissues than the non-targeted PETM Ms, thereby leading to a significantly higher antitumor activity *in vitro* and *in vivo* after encapsulated with DOX. Thus the cRGD-PETM Ms may be a promising drug nanocarrier for effective tumor therapy.

Acknowledgements

This work was supported by the National Natural Science Foundation of China (81471727, 51303213, 51203189, 81371667 and 81171371), Tianjin Science Foundation (13JCZDJC28100) and PUMC Youth Fund and the Fundamental Research Funds for the Central Universities (3332014003, 33320140034) and the Development Foundation of IRM-CAMS (SF1417 and SF1416).

Notes and references

The authors declare no competing financial interest.

[a]*Tianjin Key Laboratory of Radiation Medicine and Molecular Nuclear Medicine, Institute of Radiation Medicine, Chinese Academy of Medical Science & Peking Union Medical College. Tianjin 300192, P.R. China.*
E-mail: lewis78@163.com.
[b]*Department of Polymer Science and Technology, School of Chemical Engineering and Technology, Tianjin University, Tianjin 300072, P.R.*

China
[c] Key Laboratory of Systems Bioengineering of the Ministry of Education, Tianjin 300072, P.R. China
[d] Collaborative Innovation Center of Chemical Science and Engineering (Tianjin), Tianjin 300072, P.R. China
E-mail: ajdong@tju.edu.cn (Anjie Dong)
‡ These authors contributed equally.

1. H. Meng, M. Xue, T. Xia, Z. Ji, D. Y. Tarn, J. I. Zink and A. E. Nel, *Acs Nano*, 2011, **5**, 4131.
2. O. Veiseh, F. M. Kievit, R. G. Ellenbogen and M. Zhang, *Adv. Drug Deliv. Rev.*, 2011, **63**, 582.
3. D. Ding, Z. Zhu, R. Li, X. Li, W. Wu, X. Jiang and B. Liu, *ACS Nano*, 2011, **5**, 2520.
4. Y. Liu, L. Feng，T. Liu, L. Zhang, Y. Yao, D. Yu, L. Wang and N. Zhang, *Nanoscale*, 2014, **6**, 3231.
5. G. Gaucher, M.-H. Dufresne, V. P. Sant, N. Kang, D. Maysinger and J.-C. Leroux, *J. Control. Release,* 2005, **109**, 169.
6. E. S. Gil and S. M. Hudson, *Prog. Polym. Sci.,* 2004, **29**, 1173.
7. H. Chen, B. Li, J. Qiu, J. Li, J. Jin, S. Dai, Y. Ma and Y. Gu, *Nanoscale*, 2013, **5**, 12409.
8. K. Kataoka, A. Harada and Y. Nagasaki, *Adv. Drug Deliv. Rev.,* 2001, **47**, 113.
9. H. Cabral and K. Kataoka, *J. Control. Release,* 2014, **190**, 465.
10. N. M. Pinkerton, A. Grandeury, A. Fisch, J. Brozio, B. U. Riebesehl and R. K. Prud'homme, *Mol. Pharm.*, 2012, **10**, 319.
11. S.-M. Lee and S. T. Nguyen, *Macromolecules*, 2013, **46**, 9169.
12. J. Yue, S. Liu, R. Wang, X. Hu, Z. Xie, Y. Huang and X. Jing, *Mol. Pharm.,* 2012, **9**, 1919.
13. L. Zhang, Y. Li and C. Y. Jimmy, *J. Mater. Chem. B,* 2014, **2**, 452.
14. Y. Xiao, R. Jaskula-Sztul, A. Javadi, W. Xu, J. Eide, A. Dammalapati, M. Kunnimalaiyaan, H. Chen and S. Gong, *Nanoscale*,2012, **4**, 7185.
15. H. Wang, J. Liu, A. Han, N. Xiao, Z. Xue, G. Wang, J. Long, D. Kong, B. Liu, Z. Yang and D. Ding, *ACS Nano*, 2014, **8**, 1475.
16. Y. Duan, C. Yang, Z. Zhang, J. Liu, J. Zheng and D. Kong, *Hum. gene ther.*, 2010, **21**, 191.
17. G. Zhu, J. Zheng, E. Song, M. Donovan, K. Zhang, C. Liu and W. Tan, *Proc. Natl. Acad. Sci. U. S. A.,* 2013, **110**, 7998.
18. J. Liu, J. Liu, L. Chu, Y. Wang, Y. Duan, L. Feng, C. Yang, L. Wang and D. Kong, *Int. J. Nanomedicine,* 2011, **6**, 59.
19. S. Deshayes, H. Cabral, T. Ishii, Y. Miura, S. Kobayashi, T. Yamashita, A. Matsumoto, Y. Miyahara, N. Nishiyama and K. Kataoka, *J. Am. Chem. Soc.*, 2013, **135**, 15501.
20. C.-F. Cho, G. A. Amadei, D. Breadner, L. G. Luyt and J. D. Lewis, *Nano Lett.*, 2012, **12**, 5957.
21. X. He, M.-H. Na, J.-S. Kim, G.-Y. Lee, J. Y. Park, A. S. Hoffman, J.-O. Nam, S.-E. Han, G. Y. Sim and Y.-K. Oh, *Mol. Pharm.*, 2011, **8**, 430.
22. E. Ruoslahti, *Annu. Rev. Cell Dev. Biol.*, 1996, **12**, 697.
23. E. Koivunen, B. Wang and E. Ruoslahti, *Biotechnology*, 1995, **13**, 265.
24. J. Zhou, D. Guo, Y. Zhang, W. Wu, H. Ran and Z. Wang, *ACS Appl. Mater. Interfaces*, 2014, **6**, 5566.
25. V. Tsouris, M. K. Joo, S. H. Kim, I. C. Kwon and Y. Y. Won, *Biotechnol. Adv.*, 2014, **32**, 1037.
26. Y. Li, K. Xiao, W. Zhu, W. Deng and K. S. Lam, *Adv. Drug Deliv. Rev.,* 2014, **66**, 58.
27. J. Sankaranarayanan, E. A. Mahmoud, G. Kim, J. M. Morachis and A. Almutairi, *ACS Nano*, 2010, **4**, 5930.
28. H. Koo, M. S. Huh, I.-C. Sun, S. H. Yuk, K. Choi, K. Kim and I. C. Kwon, *Acc. Chem Res*, 2011, **44**, 1018.
29. M. Elsabahy and K. L. Wooley, *Chem. Soc. Rev.*, 2012, **41**, 2545.
30. M. Pacurari, Y. Qian, W. Fu, D. Schwegler-Berry, M. Ding, V. Castranova and N. Guo, *J. Toxicol. Environ. Health A,* 2012, **75**, 112.
31. H. Wei, R.-X. Zhuo and X.-Z. Zhang, *Prog. Polym. Sci.*, 2013, **38**, 503.
32. J. Zhao, H. Wang, J. Liu, L. Deng, J. Liu, A. Dong and J. Zhang, *Biomacromolecules*, 2013, **14**, 3973.
33. D. Crich and Q. Yao, *J. Am. Chem. Soc.,* 2004, **126**, 8232.
34. W. Chen, F. Meng, F. Li, S.-J. Ji and Z. Zhong, *Biomacromolecules*, 2009, **10**, 1727.
35. Z. Liu, M. Zheng, F. Meng and Z. Zhong, *Biomaterials*, 2011, **32**, 9109.
36. Y. Wu, W. Chen, F. Meng, Z. Wang, R. Cheng, C. Deng, H. Liu and Z. Zhong, *J. Control. Release,* 2012, **164**, 338.
37. Z. Yang, G. Liang, M. Ma, Y. Gao and B. Xu, *J. Mater. Chem.,* 2007, **17**, 850.
38. A. Liantonio, A. Accardi, G. Carbonara, G. Fracchiolla, F. Loiodice, P. Tortorella, S. Traverso, P. Guida, S. Pierno and A. De Luca, *Mol. Pharmacol.*, 2002, **62**, 265.
39. J. Zhao, J. Liu, S. Han, H. Deng, L. Deng, J. Liu, A. Meng, A. Dong and J. Zhang, *Polym. Chem.*, 2014, **5**, 1852.
40. J. Zhao, J. Liu, S. Xu, J. Zhou, S. Han, L. Deng, J. Zhang, J. Liu, A. Meng and A. Dong, *ACS Appl. Mater. Interfaces,* 2013, **5**,13216.
41. H. Deng, Y. Zhang, X. Wang, J. Zhang, Y. Cao, J. Liu, J. Liu, L. Deng, and A. Dong, *Acta Biomater.* 2015, **11**, 126.
42. L. Zhao, J. Ding, C. Xiao, P. He, Z. Tang, X. Pang, X. Zhuang, X. Chen, *J. Mater. Chem.,* 2012, **22**, 12319.
43. J. Nicolas, D. Mura S Fau - Brambilla, N. Brambilla D Fau - Mackiewicz, P. Mackiewicz N Fau - Couvreur and P. Couvreur, *Chem. Soc. Rev.,* 2013, **42**, 1147.
44. L. Chang, L. Deng, W. Wang, Z. Lv, F. Hu, A. Dong and J. Zhang, *Biomacromolecules*, 2012, **13**, 3301.
45. H. Gao, T. Cheng, J. Liu, J. Liu, C. Yang, L. Chu, Y. Zhang, R. Ma, and L. Shi, *Biomacromolecule,* 2014, **15**, 3634.
46. N. Abdullah-Al, H. Lee, Y. Lee, K. Lee, and S. Park, *Macromol. Biosci.* 2011, **11**, 1264.
47. H. Deng, J. Liu, X. Zhao, Y.Zhang, J. Liu, S. Xu, L. Kong, A. Dong, and J. Zhang, *Biomacromolecules*, 2014, **15**, 4281.
48 R. Mo, N. Sun Q Fau - Li, C. Li N Fau – Zhang and C. Zhang, *Biomaterials,* 2013, **34**, 2773.